JOURNAL OF AIRCRAFT
Vol. 29, No. 2, March–April 1992

Interference Flows Past Cylinder-Fin-Sting-Cavity Assemblies

O. Baysal* and K. Fouladi†
Old Dominion University, Norfolk, Virginia 23529
and
R. W. Leung‡ and J. S. Sheftic‡
Lockheed Missiles and Space Company, Inc., Sunnyvale, California 94089

A computer code, VISCC, is developed to solve the three-dimensional, Reynolds-averaged, unsteady, compressible, and complete Navier-Stokes equations. The equations are solved by an implicit, fully vectorized, finite-volume, upwind-biased, approximately factored, and multigrid method. A hybrid domain decomposition method is developed to utilize the combined advantages of overlapped grids, zonal grids, and block-structured grids. An algebraic turbulence model is developed to represent the Reynolds stresses. The store considered here for simulation is a missile configuration with four tail fins and an L-shaped offset sting. The missile is placed first directly above the opening of a rectangular box cavity, then submerged completely inside the cavity. These two cases represent two distinct and important interference characteristics for an internal store carriage and a subsequent separation. The freestream Mach and the unit Reynolds numbers are 2.75 and 2.97 million per foot, respectively. The results of the time-accurate computations depict these complex flows and help understanding the interference effects between the store and the cavity. These effects are more pronounced when the store is placed inside the parent body. The time-averaged surface pressures compare well with the wind-tunnel data.

Nomenclature

a	=	speed of sound, ft/s
C_N	=	normal force coefficient
E	=	inviscid flux
E_v	=	viscous flux
l	=	reference length, ft
M	=	Mach number
m	=	dummy index which takes values of 1, 2, or 3
n	=	normal unit vector
P_t	=	total pressure, psia
Q	=	conserved variables
Re	=	unit Reynolds number, million/ft
S	=	surface
T_t	=	total temperature, °R
t	=	time, s
t_c	=	time characteristic, ms
u	=	velocity, ft/s
x_1, x_2, x_3	=	Cartesian coordinates
ξ^1, ξ^2, ξ^3	=	curvilinear coordinates
Ω	=	volume

Subscript

∞	=	freestream value

Introduction

AERODYNAMIC effects of stores on a fighter or a bomber type of aircrafts and their safe operations become more important as the speed of the aircraft increases. The internal carriage of such stores is an option for a possible reduction in the aerodynamic drag and in the radar observability of certain aircraft. In addition to wind-tunnel and flight tests, computations are becoming a viable option for an internal-carriage-configuration design and its trade studies. In recent years, costs of model fabrication and the wind-tunnel tests have risen, in particular for the dynamic tests that are required for the trajectory studies or the induced flow studies. In contrast, the cost of high-speed computing with large memories has dropped and its availability has significantly increased. Computational fluid dynamics (CFD) is free from the problems of disturbing the flow with measurement probes or the wind-tunnel walls, and it can reduce risks associated with flight tests. However, it is bounded by the truncation and the round-off errors, and underlying physical assumptions.

The objective of this investigation is the application of a recently developed computational code, and to contribute to the much needed data base in understanding the interference between a parent body and a store during its separation. It is meant to augment the wind-tunnel tests, such as, those reported in Refs. 1–4. Probably, the most formidable challenges in developing the present computational method for the internal store carriage and separation have been the simulation of the complex cavity (store bay) flowfield and the grid generation for the configuration, which contains multiple and geometrically nonsimilar components. Consequently, the results being presented here have been preceded by four building-block studies: computations of cavity flows,[5–8] computations of flows past cylindrical bodies at incidence,[9–11] grid generation by a hybrid domain decomposition technique, DDT[12,13] and finally computations of interference flows past a cylinder near a flat plate.[12,14]

A two-dimensional, engineering predictive method for the store separation from a cavity is given by Culotta,[15] who uses the results from water table experiments as input to the computer code. Another predictive method is by Keen,[16] and his method uses interactively the wind-tunnel experiments for the flow angularity. Löhner[17] has shown a two-dimensional method, which solves the inviscid flow equations on unstructured grids, to simulate the separation of an object from a cavity. Promising progress to this end by various research groups is re-

Presented as Paper 90–3095 at the AIAA 8th Applied Aerodynamics Conference, Portland, OR, Aug. 20–22, 1990; received Nov. 24, 1990; revision received March 1, 1991; accepted for publication March 1, 1991.

*Associate Professor, Mechanical Engineering and Mechanics Dept. Senior Member AIAA.
†Currently at Lockheed Engineering and Sciences Company, Hampton, VA. Member AIAA.
‡Aerodynamicist, Missile Systems Division, 0/81-11. Member AIAA.

ported in several conferences on store carriage and separation held in the past three years.[3,18,19]

The present paper reports the simulation of the supersonic interference flow past a missile configuration with four fins placed near and inside a rectangular-box cavity (Fig. 1). In order to benchmark the computational method with the wind-tunnel data,[4] the L-shaped offset sting attached to the missile model is also included in this simulation. To utilize relatively less computer memory and to ease the grid generation, structured grids are used. A hybrid domain decomposition method is developed[12,13] to combine the advantages of the overlapped grids, zonal grids, and block-structured grids. As reported in Ref. 13, another demonstration of this method is performed by simulating the supersonic flow past a generic store-sting-cavity configuration, which is specifically designed for the validation of this method.[2]

Mathematical Formulation

A rectangular cavity consists of walls in all three directions. Consequently, the diffusion effects of the viscous fluxes are not negligible, and their gradients are approximately the same order of magnitude in all three directions. This requires the solution of the complete Navier-Stokes equations. Therefore, their reduced forms, such as, the thin-layer approximation or the Euler equations, produce nonphysical solutions to cavity flows. The conservative form of the nondimensional, unsteady, compressible, Reynolds-averaged, complete Navier-Stokes equations are written in the generalized curvilinear coordinates as follows:

$$\frac{\partial}{\partial \xi^1}(E - E_v)_1 + \frac{\partial}{\partial \xi^2}(E - E_v)_2 + \frac{\partial}{\partial \xi^3}(E - E_v)_3 = 0 \quad (1)$$

The effect of Reynolds stresses is incorporated through the Baldwin-Lomax algebraic turbulence model. Three specific modifications have been made to the standard Baldwin-Lomax model to account for 1) vortex-boundary-layer interaction and separation, 2) presence of multiple walls, and 3) turbulent memory effects in addition to the local equilibrium

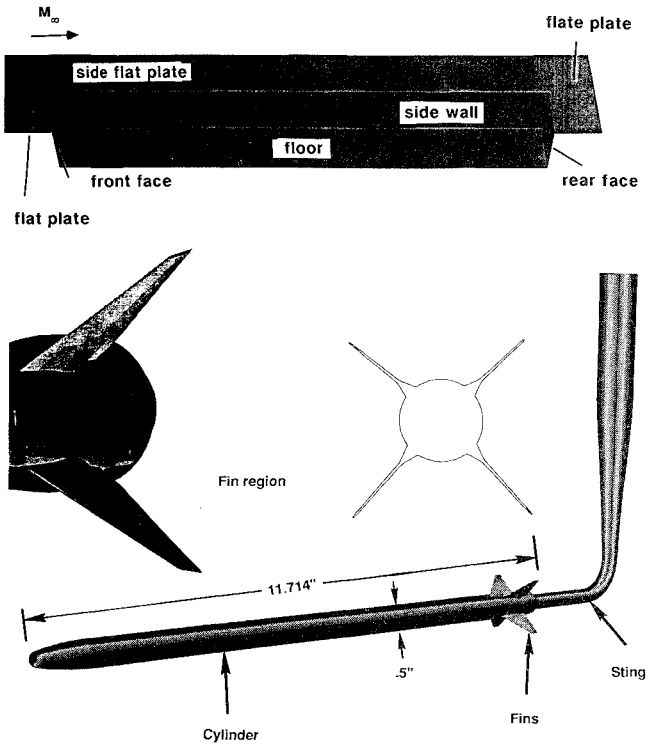

Fig. 1 Schematics of a) the rectangular-box cavity with length-to-depth ratio of 9.0; and b) the cylinder-fin-sting (CFS) assembly with fin details.

for the shear layer. Details of these modifications can be found in Refs. 6–8.

Finite-volume differencing is formulated by integrating the conservation equations [Eq. (1)] over a stationary control volume (computational domain):

$$\frac{\partial}{\partial t}\int\int\int \bar{Q}\mathrm{d}\Omega + \int\int \bar{E}\cdot\bar{n}\mathrm{d}S = 0 \quad (2)$$

Equation (2) is solved using the spatially second-order accurate method described in Refs. 8, 11, 12, 13, and 20. Either Van Leer's flux vector splitting (FVS) or Roe's flux-difference splitting (FDS) can be used to construct the upwind differences for the convective and pressure terms. Spatial derivatives are written conservatively as flux balances across each cell. The diffusion terms are centrally differenced. Spatial approximate factorization, and Euler backward integration after linearization in time, result in the solution through 5 × 5 block-tridiagonal matrix inversions in each of the three directions. When an upwind-biased approximation scheme is used, numerical oscillations are expected to appear in the presence of discontinuities. A flux limiter can be used to reduce an upwind-biased difference to a fully one-sided upwind scheme in such regions. This in turn ensures a monotonic interpolation and eliminates the overshoots and the undershoots. In the present formulation, three types of flux limiters[13] are used, where the success of each is rather case dependent.

In the present study, Roe's flux-difference-splitting (FDS) method is used to simulate the cavity flow. However, the blunt trailing edge of the curved sting and its upright position perpendicular to the freestream proves to be a difficult test for this FDS scheme. Subsequently, Van Leer's flux-vector-splitting, which is rather successful for this class of problems,[13] is used to simulate the flow about the cylinder-fin-sting assembly.

In the present algorithm, the decomposition of a flow domain into simpler subdomains is performed by employing three types of domain decomposition techniques (DDT) for structured grids. Each subdomain is chosen to ease the grid-generation task and to create a suitable mesh for the region of that particular subdomain. A proper choice of a DDT can, for example, eliminate the need for common boundaries between subdomains by using overlapped grids, or eliminate the need for interpolation at the grid interfaces by using block-structured grids, or eliminate the need for contiguous grid lines normal to the interface by using zonal grids.

The standard block or scalar tridiagonal inversion of the approximately factored, delta form of Eq. (1) can be easily extended for zonal and block-structured grids. However, due to the existence of the overlap region and the holes in the overlapped grids, substantial modifications to the solution algorithm are necessary.[21] As subdomains are moved to their overlapped positions, some cells of one grid may be found to lie inside a solid boundary contained within another grid. Also, a significant number of cells must be interpolated, if every cell common to more than one subdomain grid is to be updated. This becomes computationally expensive and it could have an adverse effect on the global accuracy when cell sizes are not compatible in different subdomain grids. This problem can be avoided by updating only the boundary of the common region between subdomains, and excluding the other cells inside this region from the calculation. This process introduces an artificial boundary or a hole inside the overset subdomain. Hence, a search method is used to create and locate these holes. Details of the DDT's used in this study and the consequent modifications to the solution algorithm are given in Refs. 12 and 13.

Configuration and Grids

The configuration for which the flow is being computed using the present method is detailed in Ref. 4. The parent body is represented by an 18-in.-long, 4-in.-wide, and 2-in.-

deep cavity centered aft of the leading edge of a 47 × 16 in. flat plate (Fig. 1a). A boundary-layer trip strip is installed 1 in. aft of the plate leading edge to promote transition to turbulent flow at the cavity lip. The store is represented by a 11.714-in. long cylinder with 0.5-in. diameter, which has a blunt-nose and a boat-tail (Fig. 1b). Four standard fins in cruciform arrangement and a curved offset sting are attached to the cylinder.

Two flow cases are picked from the large test matrix reported in Ref. 4. The cylinder axis is aligned with the longitudinal plane at the mid-span of the cavity at zero angle of attack, and 1.8 in. above the cavity opening for case 1 and 0.9 in. below the cavity opening for case 2. The positions of the store with respect to the cavity are chosen as such to illustrate two significantly different interference characteristics. Flows of both cases are assumed symmetrical, which allows the simulation of only half of the configuration. The cavity grid consists of one block above the flat plate (122 × 40 × 50) and another block inside the cavity (91 × 31 × 45), which are generated algebraically.[6-8] The grid for the cylinder-fin-sting (CFS) assembly is constructed using an algebraic-elliptic grid method.[22] After providing the surface dimensions in detail, the surface grid is generated. Then, given the surface grid and the outer boundary dimensions of the computational domain, the volume grid is generated. The grids are developed first by a transfinite interpolation method, then they are smoothed by an elliptic method (Fig. 2). The H-O grid of CFS consists of three blocks separated by the fin surfaces. The dimensions of these blocks are (121 × 17 × 41), (121 × 33 × 41), and (121 × 17 × 41).

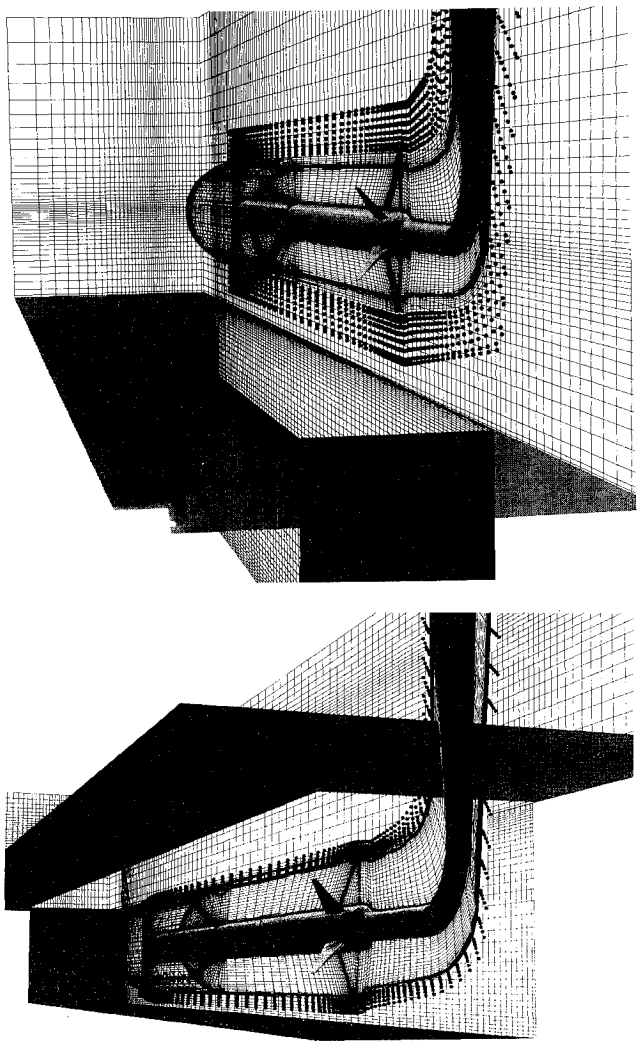

Fig. 2 Composite grid of a) CFS near the cavity (case 1); and b) CFS inside the cavity (case 2). A portion of the overlap region is marked with the circular dots.

These individually generated subdomain grids are put together to form the composite grid. The three blocks of CFS are embedded in the two blocks of cavity with overlapped intergrid volumes, thus creating holes in the cavity grids (Fig. 2). The total number of points in the composite grid is 703,332. The locations of these holes are naturally different for case 1 and case 2. Composite grids can be generated for different positions of CFS, as it moves relative to the cavity, without having to change the subdomain grids. In fact, this is one of the advantages of the present method as applied to the store separation.

The present computational method was tested earlier[13] by simulating the flow at Mach number of 1.65 past an ogive-nose-cylinder in and near a cavity with length-to-depth ratio of 6.7. This cylinder was attached to an offset sting that had a sharp leading edge and a blunt trailing edge.[2] There are major differences between the present configuration and the one considered in Refs. 2 and 13. For example, CFS has four fins, a blunt nose, and a boat tail. In comparison, an ogive-nose-cylinder with no fins was considered in Refs. 2 and 13. Shapes of the stings for these configurations are totally different. Also, the length-to-depth ratio of the present cavity is 9.0, whereas that of Refs. 2 and 13 is 6.7. Finally, the flow Mach number for the present study is relatively higher than the one considered in Refs. 2 and 13 (2.75 vs 1.65).

Boundary and Initial Conditions

Since the flow is two-dimensional on the flat plate ahead of the cavity, a two-dimensional, turbulent boundary-layer profile is generated by solving two-dimensional boundary-layer equations to match the experimentally determined thickness (0.26 in.) upstream of the cavity lip. Using this profile as an upstream boundary condition allows the computational domain to start 13 in. downstream of the flat plate leading edge, thus significant computational time and memory savings are realized. The conventional viscous flow boundary conditions, that is, no-slip, impermeability, and adiabatic-wall conditions are imposed on all solid surfaces. First-order extrapolations of the primitive variables are used at the downstream boundary. One-dimensional characteristic boundary conditions are imposed at the outer boundary and the lateral outboard boundary. Previous investigations indicated that the flowfield inside a cavity is predominantly symmetric with respect to the center plan.[6-8] The symmetry of the flow at the plane, where symmetry is assumed, is ensured by setting the contravariant velocity normal to this plane equal to zero and extrapolating the other primitive variables.

Beside the physical boundaries of the computational domain, there exist intergrid boundaries between the five subdomain grids. The conservative transfer of fluxes across a block interface, i.e., where the lines normal to the interface are contiguous, is maintained by using two sets of ghost cells on each side. Across an intergrid boundary with overlapped subdomain grids, conserved variables are interpolated nonconservatively to one set of ghost cells on each side. The coefficients of this trilinear interpolation to one grid cell are determined based on the distances to the vertices of a hexahedron formed by the cell centers of the neighboring overlapped subdomain grid.[12,13]

Since a set of coupled elliptic partial differential equations [Eq. (1)] is being solved using time-marching, the dependent variables, i.e., the conserved flow variables, need to be initialized. This can be done by either an all-quiescent domain or by an all-freestream domain. However, a more efficient method is using a fully developed solution of the empty cavity flow and a fully developed solution of the CFS flow, which are generated independently. This process is called *advanced initialization* herein. First, the governing equations are solved time accurately for the unsteady flow of the empty cavity, i.e., in the absence of the cylinder.[5-8] Any instant of this

unsteady flow can be used after the numerical transients are removed. There is no evident criterion in choosing this instant. Furthermore, since the equations are again solved to remove the numerical transients associated with the interference of the cavity and CFS, the choice of the instant for the empty cavity flow may not be important. Similarly, the CFS domain is advanced initialized with the solution for a steady flow past CFS without the cavity in its proximity.[9,11] The multigrid convergence acceleration is used in obtaining the CFS solution very efficiently.

Viscous internal store carriage code (VISCC) has been developed for this class of flows. It consists of several independent computer codes as its modules. The VISCC code is run on the Cray-2 computers of NASA Langley Research Center and Numerical Aerodynamic Simulation facility of NASA. The solver of the flow equations and the composite grid generator are called VUMXZ3 and MaGGiE, respectively. The solver VUMXZ3 is developed from the CFL3D code.[20] The CFL3D code solves the thin-layer Navier-Stokes equations on multiblock grids. The MaGGiE code is a finite volume and multigrid counterpart of the PEGSUS code.[21] The PEGSUS code can generate overlapped, finite difference grids without the multigrid convergence acceleration. The run-time memory required by VUMXZ3 for the cases being considered here is about 208 Mbytes (approximately 295 bytes per grid point). The memory requirement by each one of the other modules of VISCC is less than 70 Mbytes for these cases.

Two characteristic times are defined for two different reasons. The first characteristic time is defined as the maximum of all of the times obtained as the ratio of a cavity dimension l (reference length) to the corresponding component of the freestream velocity $t_{c1} = \max(l/u)$. It is used as a time measure for this unsteady flow. Based on the previous experience,[5-8] the numerical transients due to the nonphysical initialization of the empty cavity computational domain are assumed to be removed after running the solution algorithm for $4t_{c1}$. The

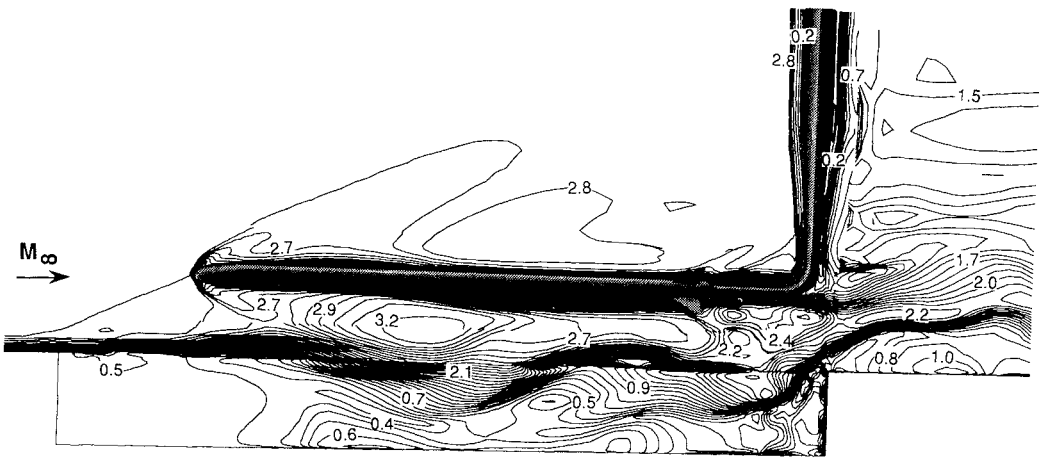

Fig. 3 Instantaneous Mach contours on the symmetry plane of case 1.

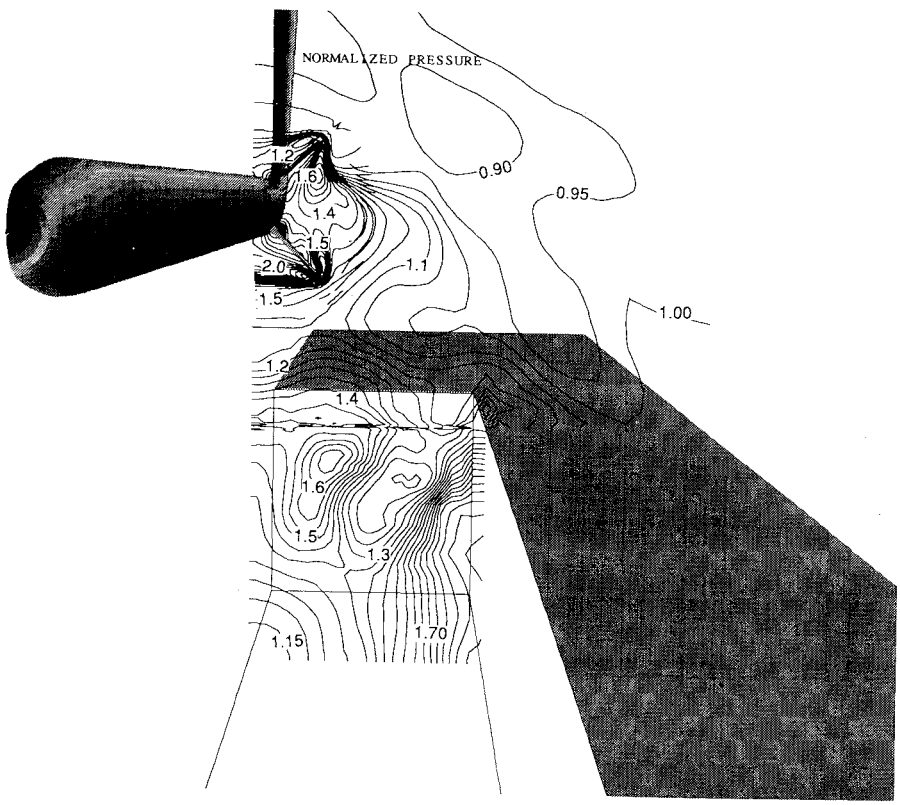

Fig. 4 Instantaneous and normalized pressure contours at a spanwise cut in the fin region of CFS for case 1.

Fig. 5 Instantaneous Mach contours of the longitudinal plane located 1.0 in. from the symmetry plane for case 1.

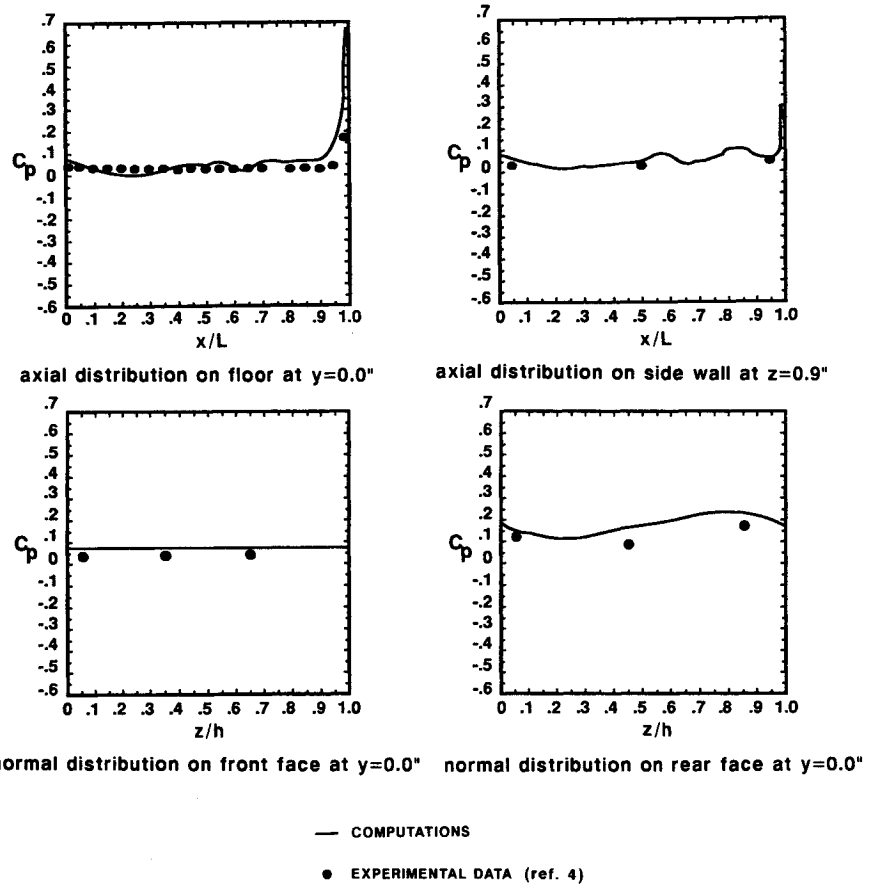

Fig. 6 Time-averaged surface pressure coefficient distributions for case 1.

second characteristic time is defined as the ratio of the minimum length of the discretization stencil, min $(5\Delta x_m)$, used by the solution algorithm to the freestream value of the speed of sound, t_{c2} = min $(5\Delta x_m)/a_\infty$. Note that this second-order algorithm uses five-point stencils in each direction. The characteristic time t_{c2} is used to determine the physical limitation set on the time step size of the solution algorithm which is advanced time accurately. To collect computational data at a rate faster than the wave propagation speed, the computational time step should be an order of magnitude less than t_{c2}. This practice ensures capturing numerically the pressure fluctuations of the cavity flow. The values of t_{c1} and t_{c2} for the present cavity are 0.73 and 0.07 ms, respectively.

The empty cavity solution is obtained for $10t_{c1}$, which requires about 25 h of computer time. The steady-state solution for the CFS in freestream is obtained by using 1 h of computer time. The interference flow solution is obtained for $2t_{c1}$ after the advanced initialization and the data is recorded for the time averaging. The computer time needed for $1t_{c1}$ of the interference flow is about 35 h. This is mainly due to the minimum step size on the CFS grid being almost an order of magnitude smaller than the minimum step size of the cavity grid. Consequently, the global time step being used is at least an order of magnitude smaller, which results in an order of magnitude more computational time per t_{c1}. The maximum CFL number is calculated to be 80.0, which also justifies using an implicit method.

The interference flows under consideration are unsteady due to fluctuations of the cavity flowfield. Therefore, neither a converged solution nor a set of criteria to signal an end to the computations exist. Although the interference flow is observed computationally in a fraction of $2t_{c1}$, this is an attempt to mimic the steady-state measurement technique of Ref. 4. The experimental data was recorded at a rate 50 times slower

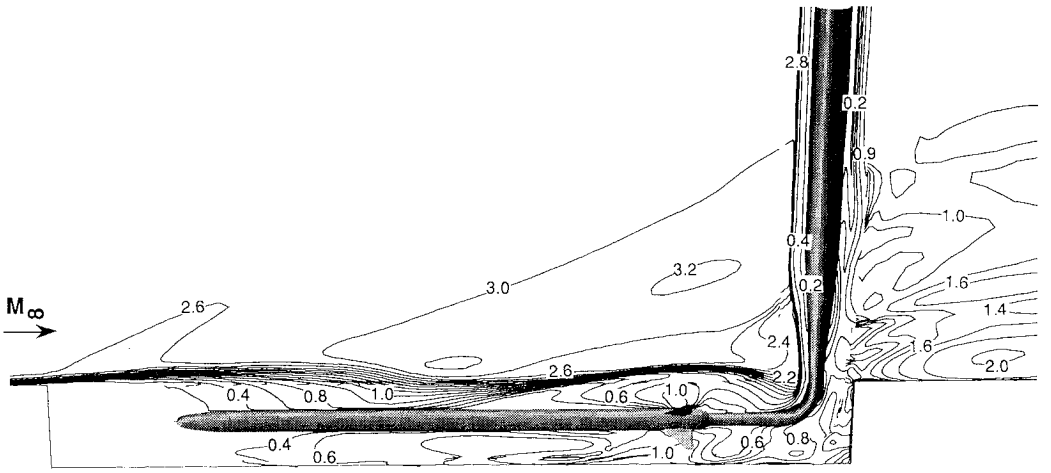

Fig. 7 Instantaneous Mach contours on the symmetry plane for case 2.

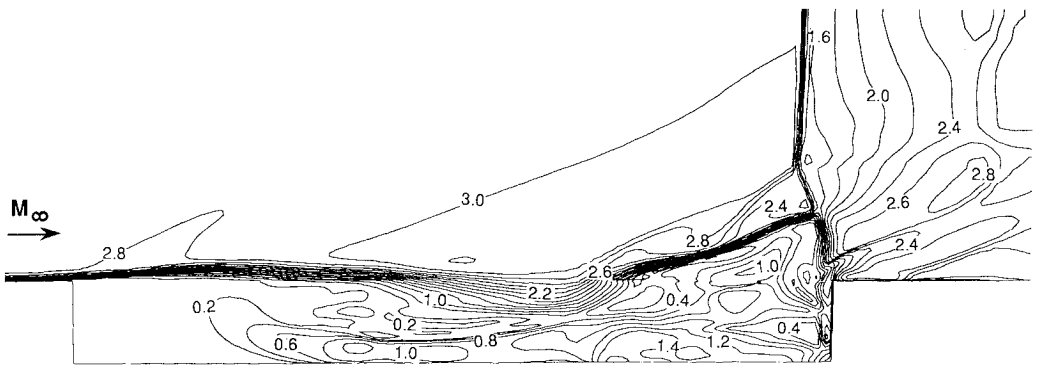

Fig. 8 Instantaneous Mach contours of the longitudinal plane located 1.0 in. from the symmetry plane for case 2.

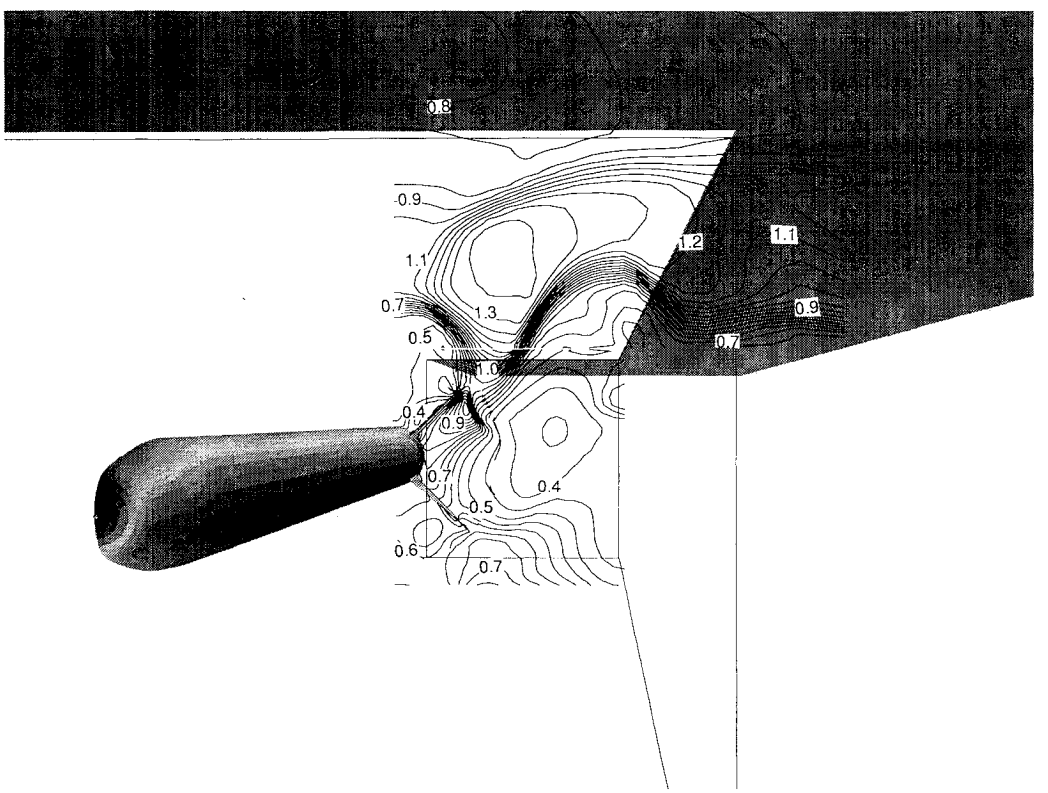

Fig. 9 Instantaneous and normalized density contours at a spanwise cut in the fin region of CFS for case 2.

than the computational rate, which is five million samples per second. The elapsed time for the experimental data averaging was five times larger than $2t_{c1}$.

Results and Discussion

The nominal wind-tunnel test conditions[4] of the turbulent flow being simulated are $M = 2.75$; $Re = 2.97$ million per foot; $P_t = 18.3$ psia; and $T_t = 580°R$. The boundary-layer thickness at the lip of the cavity is 0.26 in. The schematic of the cylinder-fin-sting (CFS) and the cavity with length-to-depth ratio of 9.0 are shown in Fig. 1. The flowfield for the instant when the CFS axis is 1.8 in. above the cavity opening, i.e., outside the cavity, is called case 1 (Fig. 2a). Case 2 is the simulation of the flowfield when the CFS axis is 0.9 in. below the cavity opening, i.e., inside the cavity (Fig. 2b). Representative results for case 1 are given in Figs. 3–6 and those for case 2 are given in Figs. 7–11.

The instantaneous Mach contours of the symmetry plane (Fig. 3) show the flow structure of case 1. As the boundary layer on the front plate separates at the front cavity lip, it forms the shear layer bridging this deep cavity. This open-type[5–7] cavity flow is predominantly transonic inside the cavity. However, the impingement of the detached shock emanating from the nose of CFS causes the shear layer to deflect inwards, creating a supersonic pocket in this region. Above this region, between the incident shock and its reflection, the Mach number is greater than its freestream value. Although it is not shown here, an observation of similar figures at various instants indicates that the shear layer and the flow inside the cavity change in time.

At the inboard and the outboard sides of CFS, boundary-layer growth is drastically different because of the cavity flow interference. Another shock structure is evident just upstream of the fins. The interaction of this shock surface and the shear layer creates a highly vortical wake just downstream of the fins. At this instant, the shear layer is deflected upward upstream of the rear cavity lip. A strong detached shock surface extends from the base to the top of the vertical sting. The wake behind this sting is highly vortical and its interaction with the shear layer clearing the cavity opening creates a complicated flow structure. The flow on the rear flat plate is partially transonic and separated. A spanwise cut of the shear layer and the flow in the fin region are depicted via the instantaneous normalized pressure contours (Fig. 4). The boundary layer on the cavity side plate reaches the shear layer through a large crossflow vortex. The elevated value of pressure inside the cavity is first reduced to the freestream value near the shear layer. As the lower surface of the inboard fin is approached, the pressure increases to its maximum value. A nonsymmetrical flow develops in the fin-to-fin region with the cylinder-inboard fin and the cylinder-outboard fin flows being significantly different.

Mach number contours of the longitudinal plane located 1.0 in. from the symmetry plane are given in Fig. 5. Since the radius of CFS is only 0.25 in., it does not appear in this figure. The flow above the shear layer is at about freestream Mach number with compression and expansion waves being created due to the undulation of the shear layer. A cross section of the strong curved shock due to the vertical sting and the wake can be seen in this figure. The flow above the rear plate has elevated Mach numbers.

Time-averaged surface pressure coefficients are plotted and compared with the wind-tunnel data[4] for various locations of the cavity (Fig. 6). The trends of the computed pressure coefficients agree with the data. It should be noted that these values vary with time for this unsteady flow. Therefore, the initial time and the elapsed time of the averaging process become variables both for the computations and the measurements. The computed values appear slightly higher than the data in Fig. 6. However, the agreement becomes better with longer elapsed times of averaging. Since the flow fluctuations are nonperiodic at supersonic speeds,[6–8] a true characteristic time for averaging is not evident. As indicated in the previous section, the empty cavity solutions are obtained for advanced initialization purposes. In comparison with the empty cavity solution, these interference results show that

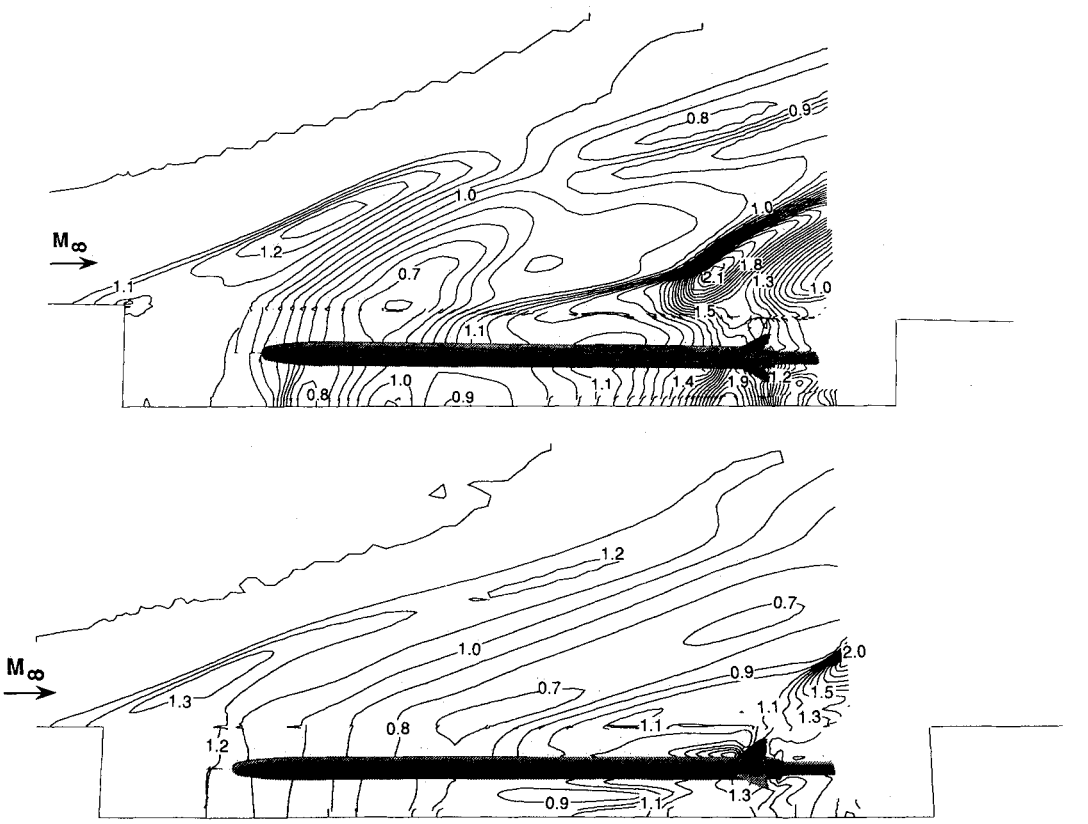

Fig. 10 Normalized pressure contours on the symmetry plane of case 2 at two different instants.

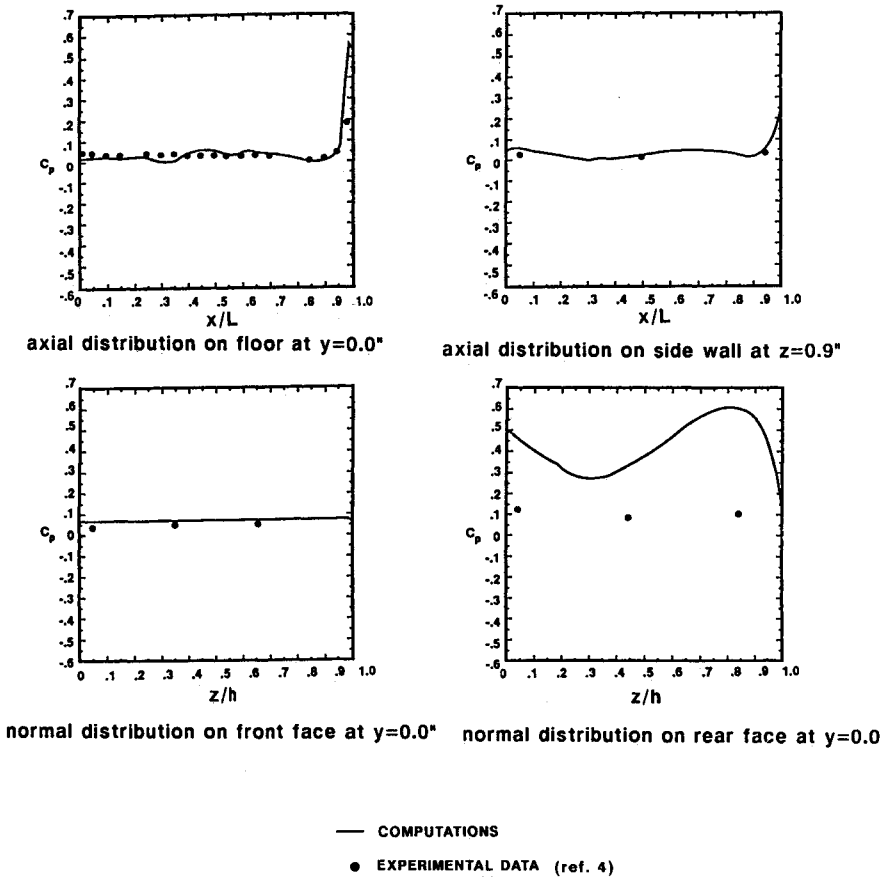

Fig. 11 Time-averaged surface pressure coefficient distributions for case 2.

CFS has a relatively smaller effect on pressure distributions over the centerline of the cavity floor. However, the differences are significant on the off-surface values of the pressure. The computational simulation of the empty cavity flow is not included herein for brevity.

The instantaneous Mach number contours of the symmetry plane (Fig. 7) depict the flow structure of case 2. The shear layer separates the supersonic external flow and the transonic internal flow by bridging the cavity. The internal flow is accelerated from the nose of CFS to the point where the shear layer impinges on the cylinder. Sonic speeds are achieved near the fin region. The shear layer interacts with the detached shock surface just ahead of the vertical sting. This interaction can be better observed with the help of instantaneous Mach number contours of longitudinal plane located 1.0 in. from the symmetry plane (Fig. 8). The shear layer, which is deflected inward in Fig. 7, is deflected up in Fig. 8. The flowfield at the fin region is depicted by the instantaneous density contours of the cross plane (Fig. 9). The shear layer is deflected inward after a large vortex near the side plate. The density values are larger around the upper fin compared to the lower fin.

Shown in Fig. 10 are the normalized pressure contours of the symmetry plane at two different instants of time. A comparison of these figures demonstrates the unsteady nature of the flowfield. Two shocks with an expansion between them are visible due to the upward deflection of the shear layer at two locations. The normalized pressure values after the first and the second shocks are about 1.3 and 2.1, respectively. At some instant later, the angle of the first shock is smaller and the second shock moves significantly in the streamwise direction. Although not shown here for brevity, observation of the flowfield plots at 20 different instants indicate nonperiodic cycles of the shock motion above the shear layer.

Finally, the time-averaged pressure coefficients on various surfaces are shown in comparison with the experimental data (Fig. 11). Generally, the trends agree well with the data except for the rear face. This may be due to the frequent impingement of the shear layer on the rear face in addition to the obvious numerical contributors, such as, the turbulence model, coarseness of the grid, and possible necessity for higher-order accuracy in time and space. The distinction between the two different interference flows considered in this study is observed in Fig. 12. Shown in this figure are the variations of the normal force coefficient C_N over a period of 1.2 ms. The mean values of C_N over this period for the store near the cavity is -0.2759 and for store inside the cavity it is 0.2912. As expected, the unsteadiness of the flow inside the cavity has a more pronounced effect on the store when it is placed inside the cavity.

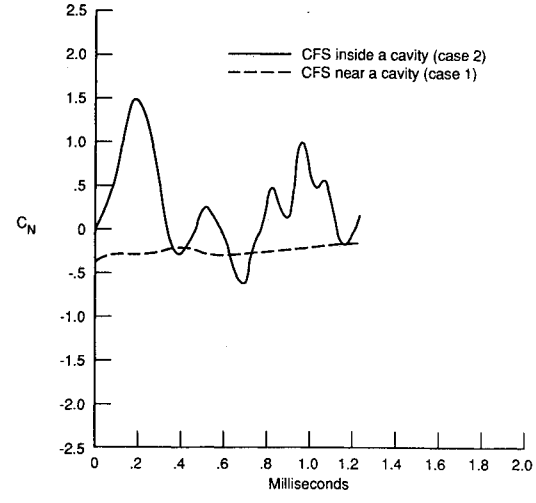

Fig. 12 Variation of C_N with time over a period of 1.2 ms for cases 1 and 2.

This study demonstrates some important fluid dynamic phenomena each of which is a topic of further and in-depth research. Among them are the supersonic shear layer, three-dimensional separations, three-dimensional vortices, shock/shear layer interaction, vortex shedding, and the wake of an upright cylinder immersed in a supersonic flow. Since these phenomena are also unsteady for the cases considered here, their structures are even more complicated.

Conclusions

The unsteady, interference flows past a cylinder-fin-sting (CFS) configuration when it is placed near and inside a cavity are computationally simulated. These two cases represent two distinct and important interference characteristics for an internal-store-carriage and a subsequent separation. This is accomplished by solving the three-dimensional, time-dependent, compressible, Reynolds-averaged, complete Navier-Stokes equations by an upwind-biased, finite-volume method. A hybrid domain decomposition method is used to ease the grid generation for this complex geometry. Favorable comparisons obtained between the computations and the experimental data contribute to the validation of the present method. Results of the present computations can contribute to the data base needed for the internal-store-carriage design and trade studies. The future work should involve the inclusion of the rigid-body dynamics into the method to study the effects of the induced flow generated by the moving store, and the investigation of the trajectory as predicted by the computed force field.

Acknowledgment

The support for this work was provided by NASA Langley Research Center and Lockheed Missiles and Space Company.

References

[1]Stallings, R. L., Jr., "Store Separation from Cavities at Supersonic Speeds," *Journal of Spacecraft and Rockets*, Vol. 20, No. 2, March–April 1983, pp. 129–132.

[2]Stallings, R. L., Jr., Wilcox, F. J., Jr., and Forrest, D. K., "Measurements of Pressures, Forces, and Moments on a Generic Store Separating From a Box Cavity at Supersonic Speeds, NASA-TP-3110, November 1991.

[3]Dix, R. E., and Butler, C., "Cavity Aeroacoustics," *Proceedings of Store Carriage, Integration and Release Conference*, Bath, U. K., The Royal Aeronautical Society, April 1990, pp. 4.1–4.34.

[4]Crosby, W. A., Carman, J. B., Hawkins, W. R., and Simons, S. A., "Store Separation Tests at Supersonic Speeds from Internal Carriage Position of a Generic Weapons Bay," Arnold Engineering Development Center, AEDC-TSR-88-V9, TN, May 1988.

[5]Baysal, O., and Stallings, R. L., Jr., "Computational and Experimental Investigation of Cavity Flowfields," *AIAA Journal*, Vol. 26, No. 1, 1988, pp. 6–8.

[6]Baysal, O., Srinivasan, S., and Stalling, R. L., Jr., "Unsteady and Viscous Calculations of Supersonic Flows Past Deep and Shallow 3-D Cavities," AIAA Paper 88-0101, Reno, NV, Jan. 1988.

[7]Srinivasan, S., and Baysal, O., "Navier-Stokes Calculations of Transonic Flows Past Cavities," *Journal of Fluids Engineering*, Vol. 113, No. 3, September 1991, pp. 300–306.

[8]Baysal, O., and Yen, G.-W., "Implicit and Explicit Computations of Flows Past Cavities With and Without Yaw," AIAA Paper 90-0049, Reno, NV, Jan. 1990.

[9]Baysal, O., and Fouladi, K., "Viscous Calculations of Supersonic Flows Past Cylinders at Angles of Attack," AIAA Paper 87-2414 CP, *Proceedings of 5th AIAA Applied Aerodynamics Conference*, Aug. 1987, pp. 338–347.

[10]Baysal, O., and Srinivasan, S., "Calculation of Wall and Free Turbulent Shear Flows at Supersonic Speeds," *Turbulent Flow Forum*, Vol. FED-51, edited by W. Bower, ASME Special Publications, June 1987, pp. 55–60.

[11]Baysal, O., Fouladi, K., and Miller, D. S., "Computation of Supersonic Flows Over a Body at High Angles of Attack," *AIAA Journal*, Vol. 27, No. 4, 1989, pp. 427–437.

[12]Baysal, O., Fouladi, K., and Lessard, V. R., "Multigrid and Upwind Viscous Flow Solver on 3-D Overlapped and Embedded Grids," *AIAA Journal*, Vol. 29, No. 6, June 1991, pp. 903–910.

[13]Fouladi, K., and Baysal, O., "Viscous Simulation Method for Flows Past a Configuration with Nonsimilar Multicomponents," *Recent Advances and Applications in CFD*, Vol. FED-103, edited by O. Baysal, ASME Special Publications, November 1990, pp. 181–190.

[14]Baysal, O., Stallings, R. L., Jr., and Plentovich, E. B., "Navier-Stokes Solutions for Store Separation and Related Problems," *Proceedings of NASA Computational Fluid Dynamics Conference*, NASA-CP-10038, Vol. 1, March 1989, pp. 385–410.

[15]Culotta, A. J., "A Predictive Technique for Determining Store Motion After Release from a Carrier Vehicle at Supersonic Speeds," AIAA Paper 86-0586, Reno, NV, Jan. 1986.

[16]Keen, K. S., "New Approaches to Computational Aircraft/Store Weapons Integration," AIAA Paper 90-0274, Reno, NV, Jan. 1990.

[17]Löhner, R., "Adaptive Remeshing for Transient Problem with Moving Bodies," AIAA Paper 88-3736 CP, June 1988.

[18]*Proceedings of Workshops on Weapons Carriage and Separation*, Second, Wright-Patterson AFB, OH, April 1988; Third, Naval Air Development Center, Warminster, PA, April 1989.

[19]*Proceedings of Eighth JOCG Aircraft/Stores Compatibility Symposium*, Armament Laboratory, Eglin AFB, FL, Oct. 1990.

[20]Thomas, J. L., Taylor, S. L., and Anderson, W. K., "Navier-Stokes Computations of Vortical Flows Over Low Aspect Ratio Wings," AIAA Paper 87-0207, Reno, NV, Jan. 1987.

[21]Steger, J. L., Dougherty, F. C., and Benek, J. A., "A Chimera Grid Scheme," *Advances in Grid Generation*, Vol. FED-5, edited by K. Ghia, ASME Special Publications, June 1983, pp. 59–69.

[22]Thompson, J. F., Lijewski, L. E., and Gatlin, B., "Efficient Application Techniques of the EAGLE Grid Code to Complex Missile Configurations," AIAA Paper 89-0361, Reno, NV, Jan. 1989.